Calculating QCD Phase Diagram Trajectories of Nuclear Collisions using a Semi-analytical Model

Todd Mendenhall¹ and Zi-Wei Lin¹

¹Department of Physics, East Carolina University, Greenville, NC 27858

Abstract. At low to moderate collision energies where the parton formation time τ_F is not small compared to the nuclear crossing time, the finite nuclear thickness significantly affects the energy density $\epsilon(t)$ and net conserved-charge densities such as the net-baryon density $n_B(t)$ produced in heavy ion collisions. As a result, at low to moderate energies the trajectory in the QCD phase diagram is also affected by the finite nuclear thickness. Here, we first discuss our semi-analytical model and its results on $\epsilon(t)$, $n_B(t)$, $n_Q(t)$, and $n_S(t)$ in central Au+Au collisions. We then compare the T(t), $\mu_B(t)$, $\mu_Q(t)$, and $\mu_S(t)$ extracted with the ideal gas equation of state (EoS) with quantum statistics to those extracted with a lattice QCD-based EoS. We also compare the $T-\mu_B$ trajectories with the RHIC chemical freezeout data. Finally, we discuss the effect of transverse flow on the trajectories.

1 Introduction

The Bjorken energy density formula [1] predicts the energy density in the central spacetime rapidity region produced in the initial state of heavy ion collisions assuming that partons originate at $(z_0, t_0) = (0, 0)$. After averaging over the transverse overlap area $A_{\rm T}$ (where we take the radius $R_A = 1.12A^{1/3}$ fm from the hard-sphere model), one needs to take a finite initial time because the Bjorken energy density formula diverges as $t \to 0$:

$$\epsilon^{Bj}(t) = \frac{1}{t A_{\rm T}} \frac{dE_{\rm T}}{du}.$$
 (1)

Here, dE_T/dy is the transverse energy rapidity density at mid-rapidity. A similar formula can be used to calculate the net-baryon density as a function of time [2]:

$$n_{\rm B}^{\rm Bj}(t) = \frac{1}{t \, A_{\rm T}} \frac{dN_{\rm netB}}{du},\tag{2}$$

which depends on the net-baryon rapidity density at midrapidity $dN_{\rm netB}/dy$. In Eqs. (1)-(2), the peak density occurs at the earliest time, which we take as the parton proper formation time $\tau_{\rm F}$.

In our semi-analytical model [3], we neglect secondary parton interactions and consider that produced partons are free-streaming, like the Bjorken energy density formula of Eq. (1). However, we include the finite nuclear thickness by considering the finite time x and longitudinal width z_0 of the primary NN collisions, and obtain for the energy density:

$$\epsilon(t) = \frac{1}{A_{\rm T}} \iint_{S} \frac{dx \, dz_0}{t - x} \frac{d^3 m_{\rm T}}{dx \, dz_0 \, dy} \cosh^3 y. \tag{3}$$

We then simplify the above integral by assuming that $d^3m_{\tau}/(dx\,dz_0\,dy) \propto dm_{\tau}/dy$, i.e., the initial transverse

mass rapidity density is uniformly distributed over the initial production area S in the $x-z_0$ plane [3]. Note that $dm_{\rm T}/dy = dE_{\rm T}/dy + m_{\rm N}dN_{\rm netB}/dy$ where $m_{\rm N}$ is the nucleon mass. Recently, we have further extended our semi-analytical model [2] to calculate the net conserved-charge densities including the net-baryon density $n_{\rm n}(t)$ as

$$n_{\rm B}(t) = \frac{1}{A_{\rm T}} \iint_{S} \frac{dx \, dz_0}{t - x} \frac{d^3 N_{\rm netB}}{dx \, dz_0 \, dy} \cosh^2 y.$$
 (4)

Since the initial net-charge comes from incoming protons and there is no net-strangeness in the incoming nuclei, the net-electric charge and net-strangeness densities in our semi-analytical model are respectively given by

$$n_{Q}(t) = n_{B}(t)\frac{Z}{A}$$
, and $n_{S}(t) = 0$. (5)

Using the densities from our semi-analytical model, the temperature T(t) and chemical potentials $\mu(t)$ can then be extracted for the ideal gas EoS with quantum statistics with the following relations [2]:

$$\begin{split} \epsilon &= \frac{19\pi^2}{12} T^4 + 3 \frac{(\mu_{\rm B} - 2\mu_{\rm S})^2 + \mu_{\rm S}^2}{2} T^2 + 3 \frac{(\mu_{\rm B} - 2\mu_{\rm S})^4 + \mu_{\rm S}^4}{4\pi^2}, \\ n_{\rm B} &= \frac{\mu_{\rm B} - \mu_{\rm S}}{3} T^2 + \frac{(\mu_{\rm B} - 2\mu_{\rm S})^3 + \mu_{\rm S}^3}{3\pi^2}, \\ n_{\rm Q} &= \frac{2\mu_{\rm B} - 5\mu_{\rm S}}{3} T^2 + \frac{2(\mu_{\rm B} - 2\mu_{\rm S})^3 - \mu_{\rm S}^3}{3\pi^2}. \end{split} \tag{6}$$

In the above, we assume that the quark-gluon plasma (QGP) consists of massless gluons and quarks, and we have used the fact that $n_{\rm s}(t)=0$ for the ideal gas EoS leads to $\mu_{\rm Q}=\mu_{\rm B}-3\mu_{\rm s}$. Therefore, the problem of extracting a $T-\mu_{\rm B}$ trajectory in the QCD phase diagram is reduced from solving a system of four equations with four unknowns to solving the above system of three equations with three unknowns.

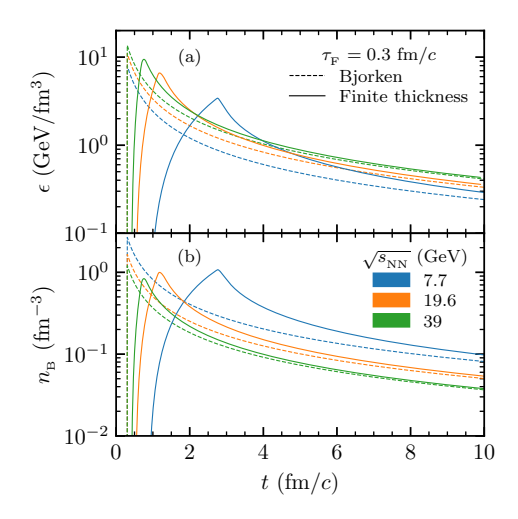


Figure 1. (a) $\epsilon(t)$ and (b) $n_{\rm B}(t)$ at mid-spacetime-rapidity from the Bjorken formula (dashed) and our formula (solid) for central Au+Au collisions at $\sqrt{s_{\rm NN}}=7.7,\ 19.6,\ {\rm and}\ 39\ {\rm GeV}$ with $\tau_{\rm F}=0.3\ {\rm fm/c}$.

One can also use a lattice QCD-based EoS to extract the $T, \mu_{\rm B}, \mu_{\rm Q}, \mu_{\rm S}$ from $\epsilon, n_{\rm B}, n_{\rm Q}, n_{\rm S}$, where these quantities are related with the standard thermodynamic relations [4]. Each of the conserved-charge densities n and the entropy density s are given by a derivative of the pressure p:

$$\begin{split} \frac{\epsilon}{T^4} &= \frac{s}{T^3} - \frac{p}{T^4} + \frac{\mu_{\rm B}}{T} \frac{n_{\rm B}}{T^3} + \frac{\mu_{\rm Q}}{T} \frac{n_{\rm Q}}{T^3} + \frac{\mu_{\rm S}}{T} \frac{n_{\rm S}}{T^3}, \\ \frac{n_{\rm B}}{T^3} &= \frac{1}{T^3} \frac{\partial p}{\partial \mu_{\rm B}} \bigg|_{T,\mu_{\rm Q},\mu_{\rm S}}, \quad \frac{n_{\rm Q}}{T^3} &= \frac{1}{T^3} \frac{\partial p}{\partial \mu_{\rm Q}} \bigg|_{T,\mu_{\rm B},\mu_{\rm S}}, \\ \frac{n_{\rm S}}{T^3} &= \frac{1}{T^3} \frac{\partial p}{\partial \mu_{\rm S}} \bigg|_{T,\mu_{\rm B},\mu_{\rm Q}}, \quad \frac{s}{T^3} &= \frac{1}{T^3} \frac{\partial p}{\partial T} \bigg|_{\mu_{\rm B},\mu_{\rm Q},\mu_{\rm S}}. \end{split} \tag{7}$$

In the above, the pressure p is defined by a Taylor series in powers of μ/T up to total power $i + j + k \le 4$:

$$\frac{p(T, \mu_{\rm\scriptscriptstyle B}, \mu_{\rm\scriptscriptstyle Q}, \mu_{\rm\scriptscriptstyle S})}{T^4} = \sum_{i,j,k} \frac{1}{i! \ j! \ k!} \chi^{BQS}_{ijk} \left(\frac{\mu_{\rm\scriptscriptstyle B}}{T}\right)^j \left(\frac{\mu_{\rm\scriptscriptstyle Q}}{T}\right)^j \left(\frac{\mu_{\rm\scriptscriptstyle S}}{T}\right)^k, \quad (8)$$

where the coefficients χ^{BQS}_{ijk} are parameterized as functions of T [4] based on lattice QCD results.

2 Results

In Fig. 1, we show the time evolution of the energy density $\epsilon(t)$ and net-baryon density $n_{\rm B}(t)$ calculated with Eqs. (3)-(4) from our semi-analytical model compared to those calculated with the Bjorken formulas of Eqs. (1)-(2). The results are for central Au+Au collisions at $\sqrt{s_{\rm NN}}=7.7$, 19.6, and 39 GeV for a parton formation time of $\tau_{\rm F}=0.3$ fm/c. As $\sqrt{s_{\rm NN}}$ increases, the maximum energy density $\epsilon^{\rm max}$ in Fig. 1 increases while the maximum net-baryon

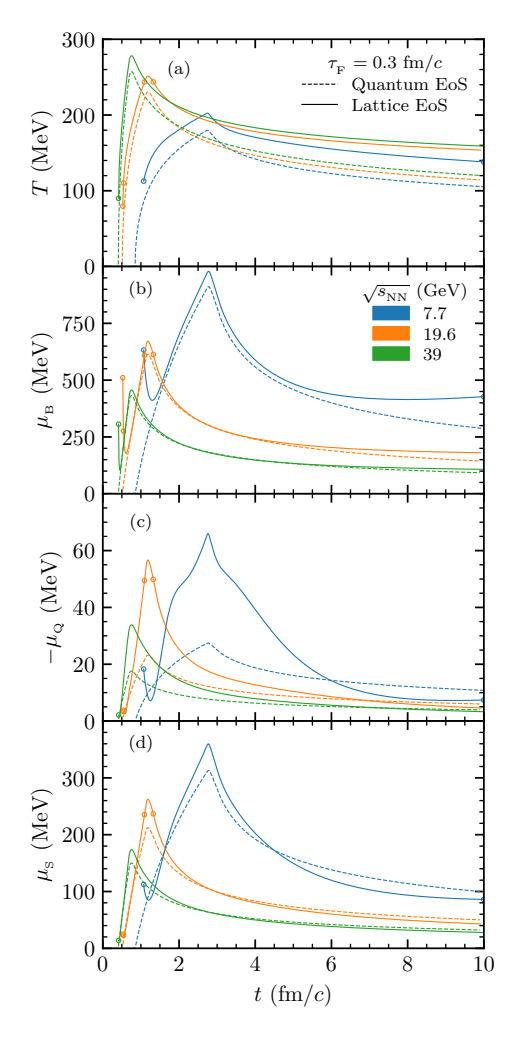


Figure 2. (a) T(t), (b) $\mu_{\rm B}(t)$, (c) $-\mu_{\rm Q}(t)$, and (d) $\mu_{\rm S}(t)$ extracted with the quantum EoS (dashed) and the lattice EoS (solid) for central Au+Au collisions at $\sqrt{s_{\rm NN}}=7.7$, 19.6, and 39 GeV with $\tau_{\rm F}=0.3$ fm/c. Open circles on the lattice EoS curves represent times when $\mu_{\rm B}/T>2.5$.

density $n_{\rm B}^{\rm max}$ decreases according to our semi-analytical model. While $\epsilon^{\rm max}$ also increases with $\sqrt{s_{\rm NN}}$ according to the Bjorken formula, it occurs at $t=\tau_{\rm F}$ whereas $\epsilon^{\rm max}$ from our semi-analytical model occurs later, at time $t\in[t_a,t_2+\tau_{\rm F}]$ [2]. Note that t_1 and t_2 represent the starting and ending time of the nuclear overlap, respectively; the nuclear crossing time is $d_t=2R_{\rm A}/(\beta\gamma)$, and we choose $t_1=d_t/6$ and $t_2=5d_t/6$ [2].

We also see in Fig. 1 that for both the Bjorken formula and our semi-analytical model, $n_{\rm B}^{\rm max}$ decreases with $\sqrt{s_{\rm NN}}$ and it is reached at the same time as $\epsilon^{\rm max}$. One major difference between the Bjorken formulas and our semi-analytical model is that our densities start at zero (at

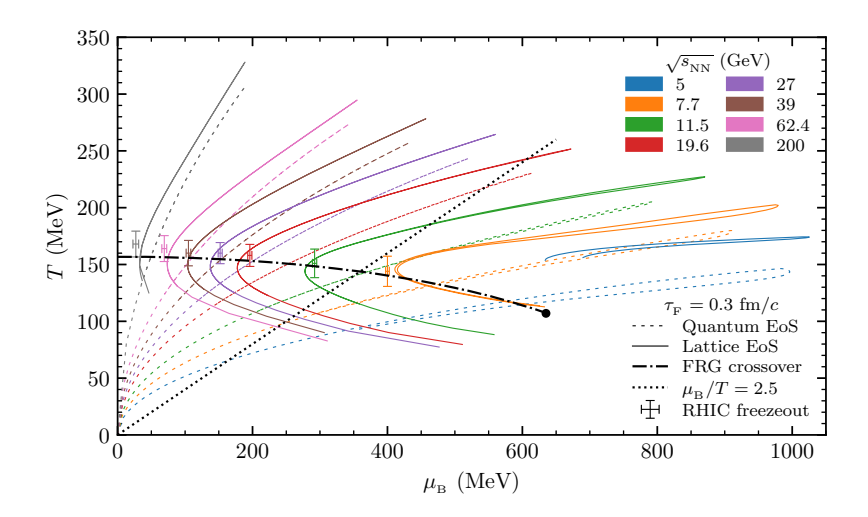


Figure 3. QCD phase diagram trajectories extracted with the quantum EoS (dashed) and the lattice EoS (solid) compared with the RHIC chemical freezeout data (symbol with error bars) for central Au+Au collisions at $\sqrt{s_{\text{NN}}} = 5.0, 7.7, 11.5, 19.6, 27, 39, 62.4$, and 200 GeV with $\tau_{\text{F}} = 0.3$ fm/c. The FRG crossover curve (dot-dashed) with the CEP and the $\mu_{\text{B}}/T = 2.5$ line are also shown for reference.

 $t=t_1+\tau_{\rm F}$), increase to their maximum values, then decrease thereafter. On the other hand, Bjorken densities start at their maximum values and decrease with time. We also find that the late time evolution of our densities approaches that of the Bjorken formula. This occurs because the formed partons in our model must have $y\sim 0$ in order to contribute to the densities in the mid-spacetime-rapidity region at late times, just like the Bjorken formula.

Figure 2 shows the time evolution of the temperature T(t) and chemical potentials $\mu(t)$ for the quantum EoS and the lattice EoS extracted using our densities at $\sqrt{s_{NN}}$ = 7.7, 19.6, and 39 GeV with $\tau_{\rm F} = 0.3$ fm/c. For both equations of state, we extract the $T, \mu_{\rm B}, \mu_{\rm O}$, and $\mu_{\rm S}$ using the conditions in Eq.(5) from our semi-analytical model, which are relevant for heavy ion collisions and have also been used to constrain the lattice EoS [4]. As $\sqrt{s_{_{NN}}}$ increases, the maximum temperature T^{max} increases, but the maximum baryon chemical potential $\mu_{\scriptscriptstyle \rm B}^{\rm max}$ decreases in Fig. 2. The results for the lattice EoS show that $\mu_{\rm B}$ first decreases before increasing with time, because the lattice EoS smoothly merges with the hadron resonance gas model at $T \lesssim 135 \text{ MeV}$ [4]. The open circles in Fig. 2 represent the times when the lattice trajectories are inside the region $\mu_{\rm B}/T > 2.5$, where the lattice EoS is expected to break down [4]. We also observe in Fig. 2(c) that μ_0^{max} from the lattice EoS can be much larger than that from the quantum EoS (by a factor \sim 2), while in Fig.2(d) the $\mu_{\rm s}^{\rm max}$ values extracted from the two EoS are reasonably close (within $\sim 20\%$ of each other). Note that a recent work [5] using the AMPT model, which includes secondary parton interactions, found similar results for the time dependences of T and μ as our results here.

In Fig. 3, we show the trajectories extracted from our densities using the quantum and lattice equations of state

in comparison with the RHIC chemical freezeout data, which were obtained from grand canonical fits to the particle yields [6]. Trajectories for energies $\sqrt{s_{\rm NN}}=7.7,\,11.5,\,19.6,\,27,\,39,\,62.4,$ and 200 GeV with $\tau_{\rm F}=0.3\,$ fm/c cross the crossover curve and can thus be compared with the freezeout data, while the $\sqrt{s_{\rm NN}}=5.0\,$ GeV lattice trajectory indicates a problem in finding the full $T-\mu_{\rm B}$ solution. We can see the effect of using the more realistic lattice EoS on the extracted trajectories; e.g., the intersections with the crossover curve from the functional renormalization group (FRG) [7] shift to smaller $\mu_{\rm B}$ and are closer to the RHIC chemical freezeout data.

The maximum temperature reached by the trajectories extracted with the lattice EoS are also larger than that extracted with the quantum EoS, which is also shown in Fig. 2. In addition, $\mu_{\rm B}^{\rm max}$ extracted with the lattice EoS is significantly larger ($\sim 10\%$) at low to moderate collision energies than that with the quantum EoS. As $\sqrt{s_{\rm NN}}$ increases, the difference in $\mu_{\rm B}^{\rm max}$ between the two equations of state becomes smaller such that there is essentially no difference at $\sqrt{s_{\rm NN}}=200$ GeV. Note that the lattice trajectories at late times below the FRG crossover curve do not approach the origin but instead go to a finite $\mu_{\rm B}$ and low T in the QCD phase diagram. This behavior can also be seen in Fig. 2(b), where $\mu_{\rm B}$ at late times can increase when using the lattice EoS but always decreases when using the quantum EoS.

In order to extract the lattice EoS trajectories in Fig. 3, we calculate the intersection points between the constant ϵ and $n_{\rm B}$ contours in the $T-\mu_{\rm B}$ plane that correspond to the $\epsilon(t)$ and $n_{\rm B}(t)$ values at a given time t from our model [2]. We find that the lattice EoS does not have $T-\mu_{\rm B}$ solutions for low collision energies at very early or very late times; this usually happens when the trajectory is in the

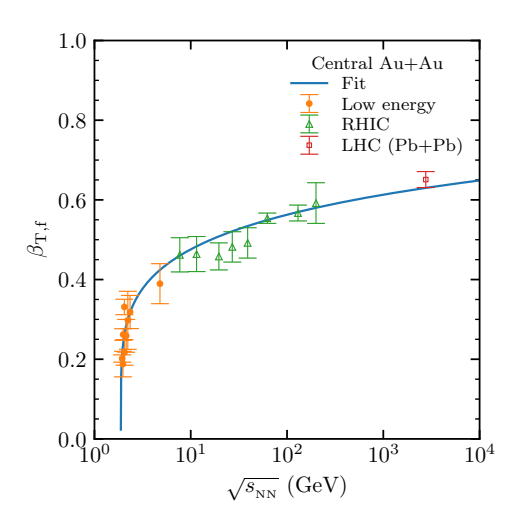


Figure 4. Our parameterization (solid) of the final transverse velocity $\beta_{T,I}$ in central Au+Au collisions as a function of collision energy compared to kinetic freezeout values from multiple low energy experiments (circles), the Beam Energy Scan program at RHIC (triangles), and the LHC (square).

large $\mu_{\rm B}/T$ region where the lattice EoS is expected to be unreliable [4]. For example, the $\sqrt{s_{\rm NN}}=5.0$ GeV lattice trajectory in Fig. 3 has no $T-\mu_{\rm B}$ solution below the FRG crossover line for the densities from our semi-analytical model. Moreover, we find that no solution exists in the lattice EoS for our densities at any time in the evolution of central Au+Au collisions at $\sqrt{s_{\rm NN}}=2.0$ GeV [2]. Therefore, the lattice EoS is an improvement over the ideal gas EoS at high collision energies where $\mu_{\rm B}/T<2.5$; however, it is expected to be unreliable at low energies.

We have also investigated the effect of transverse expansion by increasing the transverse overlap area $A_{\rm T}$ with time t in Eqs. (3)-(4). The transverse radius $R_{\rm T}$ of the overlap region increases according to a data-based parameterization of the transverse flow velocity $\beta_{\rm T}(t)$. We assume that $\beta_{\rm T}(t)$ starts at 0 and smoothly approaches a final value $\beta_{\rm T,f}$. Using the kinetic freezeout data, which were obtained by fitting the transverse momentum spectra of central Au+Au collisions at various collision energies [6] to a blast-wave model, we parameterize $\beta_{\rm T,f}$ as [2]:

$$\beta_{\text{T,f}} = \left[\frac{\ln\left(\sqrt{s_{\text{NN}}}/E_0\right)}{64.7 + \ln\left(\sqrt{s_{\text{NN}}}/E_0\right)} \right]^{0.202},\tag{9}$$

where $E_0 = 2m_{\rm N}$ is the threshold energy. Figure 4 shows the parameterization in comparison with the kinetic freezeout data [6]. The data at low energies (orange circles) and RHIC energies (green triangles) are for Au+Au collisions, while the data at the LHC energy (red square) is for Pb+Pb collisions at 2.76 TeV (where we have ne-

glected the difference between Pb and Au for the kinetic freezeout data).

Further details regarding the implementation and effects of transverse expansion in our semi-analytical model can be found in the full study [2]. Overall, we find that including the transverse flow essentially does not change the path of the trajectory (at a given $\sqrt{s_{\rm NN}}$ and $\tau_{\rm F}$), but it moves the trajectory endpoint, the $T-\mu_{\rm B}$ point corresponding to $\epsilon^{\rm max}$ and $n_{\rm B}^{\rm max}$, a bit closer to the origin. Importantly, the transverse expansion significantly decreases the time spent in the parton phase (i.e., the QGP lifetime) at all collision energies, and we also find that the QGP lifetime may have a local maximum below $\sqrt{s_{\rm NN}}\sim 11.5$ GeV [2].

3 Summary and Outlook

In this proceeding, we have calculated the $T - \mu_{\rm B}$ trajectories in the QCD phase diagram for central Au+Au collisions using our semi-analytical model, which includes the effect of the finite nuclear thickness. have shown how the trajectories depend on the chosen equation of state and that the trajectories extracted with a lattice QCD-based EoS agree rather well with the chemical freezeout data from the RHIC Beam Energy Scan program. We also briefly discuss the implementation of transverse expansion and its effects on the trajectories. We have written a web interface [8], which currently calculates the densities and trajectories after the user specifies the colliding nuclei, $\sqrt{s_{_{
m NN}}}$, $au_{_{
m F}}$, and the ideal gas EoS with quantum or Boltzmann statistics. We plan to further improve this web interface to include options to use the lattice EoS and/or consider transverse expansion. We hope that our semi-analytical model provides a useful tool for exploring the evolution of the dense matter in the QCD phase diagram.

This work has been supported by the National Science Foundation under Grant No. PHY-2012947.

References

- [1] J.D. Bjorken, Phys. Rev. D 27, 140 (1983)
- [2] T. Mendenhall, Z.W. Lin (2021), 2111.13932
- [3] T. Mendenhall, Z.W. Lin, Phys. Rev. C 103, 024907 (2021)
- [4] J. Noronha-Hostler, P. Parotto, C. Ratti, J.M. Stafford, Phys. Rev. C 100, 064910 (2019)
- [5] H.S. Wang, G.L. Ma, Z.W. Lin, W.j. Fu, Phys. Rev. C 105, 034912 (2022)
- [6] L. Adamczyk et al. (STAR), Phys. Rev. C 96, 044904 (2017)
- [7] W.j. Fu, J.M. Pawlowski, F. Rennecke, Phys. Rev. D 101, 054032 (2020)
- [8] A web interface that performs our semianalytical calculations is availabe at http://myweb.ecu.edu/linz/densities/ (2021)